

See discussions, stats, and author profiles for this publication at: <https://www.researchgate.net/publication/272842463>

Computational and Experimental Investigation of the Optical Properties of the Chromene Dyes

ARTICLE *in* THE JOURNAL OF PHYSICAL CHEMISTRY A · FEBRUARY 2015

Impact Factor: 2.69 · DOI: 10.1021/acs.jpca.5b00394 · Source: PubMed

READS

123

7 AUTHORS, INCLUDING:



Boris Minaev

Черкаський національний університет

327 PUBLICATIONS 3,188 CITATIONS

[SEE PROFILE](#)



Rashid Valiev

Tomsk State University

22 PUBLICATIONS 86 CITATIONS

[SEE PROFILE](#)



Ruslan Magomedtakhirovich Gadirov

Tomsk State University

38 PUBLICATIONS 57 CITATIONS

[SEE PROFILE](#)

Computational and Experimental Investigation of the Optical Properties of the Chromene Dyes

Boris F. Minaev,^{†,‡} Rashid R. Valiev,^{*,†,§} Elena N. Nikonova,[†] Ruslan M. Gadirov,[†] Tatyana A. Solodova,[†] Tatyana N. Kopylova,[†] and Eugene N. Tel'minov[†]

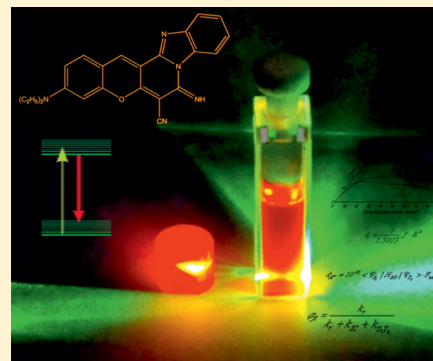
[†]Department of Optics and Spectroscopy, Tomsk State University, 36 Lenin Avenue, 634050, Tomsk, Russia

[‡]Bohdan Khmelnytsky National University, Cherkassy, 18031, Ukraine

[§]Tomsk Polytechnic University, 30 Lenin Avenue, 634050, Tomsk, Russia

S Supporting Information

ABSTRACT: Absorption and fluorescence spectra of the chromene 3 and chromene 13 dyes are studied experimentally and by density functional theory (DFT) including vibronic structure analysis. Vertical electronic absorption spectra are also calculated with the *ab initio* multiconfiguration method XMC-QDTP2. The vibronic progression for the $S_0 \rightarrow S_1$ electronic transition is calculated within the Franck–Condon approximation including Dushinsky effect and promoting modes are analyzed. The laser-active solid-state media with high efficiency and long operation time are created implementing the studied dyes. The results of investigation indicate that the studied compounds can be used as effective laser dyes in the red range of visible light.



I. INTRODUCTION

The solid active media of tunable lasers possess the high-quality emission characteristics and provide the ability to operate in various excitation modes. High reliability, stability and compactness of these devices lead to their potential usage in various fields of science, medicine, industry, communications, etc. During last years the number of active solid-state media were developed which emit light in a wide range of the electromagnetic spectrum.^{1–8} It should be noted, that the most advanced lasers based on organic solid-state active media, for instance, coumarines, at present, emit in the blue-green region of the visible light spectrum.^{1–4} In recent time a number of solid active media based on the BODIPY,^{9–16} perylene,^{17,18} rhodamine^{19–21} dyes and dye-doped matrices with silica-containing polymers,^{22,23} and hybrid matrices,^{24,25} emitting in the orange and red regions have been successfully developed.^{5–24} It is well-known that just the emission in the red range of the spectrum can deeply penetrate into biological tissues. Therefore, the creation of solid-state active medium emitting in this spectral range is a vital necessity in applied medicine.

At present, the 3-(diethylamino)-7-oxo-7*H*-benzo[4,5]-imidazo[1,2-*a*]chromeno[3,2-*c*]pyridine-6-carbonitrile dye (chromene 3) and the 3-(diethylamino)-7-imino-7*H*-benzo[4,5]-imidazo[1,2-*a*]chromeno[3,2-*c*]pyridine-6-carbonitrile dye (chromene 13) are utilized in the coloring plastics and synthetic fabrics (Figure 1). Their trade names are Solvent Red 197 and Solvent Red 196 (CAS 52372-39-1 and 52372-36-8), respectively, being widely used for industrial coloring engineering plastics²⁶ and as luminescent probes.²⁷ These compounds

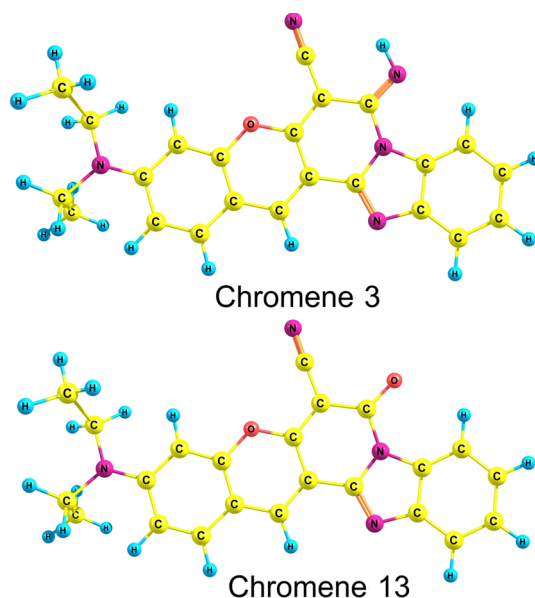


Figure 1. Equilibrium geometry of the ground electronic state of the considered molecules.

were also investigated in the form of active media in order to implement them as a tunable laser in the methanol solvent with

Received: January 14, 2015

Revised: February 23, 2015



ACS Publications

© XXXX American Chemical Society

A

DOI: 10.1021/acs.jpca.5b00394
J. Phys. Chem. A XXXX, XXX, XXX–XXX

a wide tunable region (70 nm).²⁸ The results of these studies indicate a good prospect of the laser-active media creation based on these dyes. One should note that despite the fact that these compounds are well-known for a long time, their spectral-luminescent and lasing properties were not studied in a comprehensive form with a proper theoretical backgrounds.

In the present work the spectral, photophysical and lasing properties of the considered chromene dyes in organic solvents were investigated using experimental and *ab initio* theoretical methods. Also, the solid-state active media with the high laser efficiency were synthesized. The created materials can be used in medicine as a source of the red laser emission.

II. EXPERIMENTAL AND CALCULATION DETAILS

A. Experiment. The absorption and fluorescence spectra of both chromene dyes in ethanol solution were measured using spectrofluorimeter-spectrophotometer CM2203 (Solar). Their lasing spectra were studied using the CCD-spectrometer AvaSpec-ULS2048 (Avantes) at a pulsed pumping regime of the second harmonic of YAG Nd³⁺ laser ($\lambda = 532$ nm, $\tau = 10$ ns). The pump energy and the lasing emission were controlled by the Gentec DUO and Ophir NOVA II energy measurer devices with the piezoelectric heads. Concentration of the considered dye substance in solution was 2×10^{-4} mol/L. The pumping was carried out with the transversely embodiment in a nonselective resonator with a base of 3 cm. The resonator was formed by hollow aluminum mirror (reflection $R = 95\%$) and the wall of the cuvette ($R = 5\%$) or by the solid-state active media. The laser beam was focused at the wall of cuvette or solid-state active medium using an aperture and cylindrical lenses in a strip of the size 10×0.3 mm. The density of the pump power was varied from 0.5 to 80 MW/cm² using a neutral density filters.

B. Theory. The equilibrium geometries of the electronic ground state (S_0) and of the first singlet excited (S_1) state of the studied dyes were optimized at the DFT level and at the time-depend (TD) density functional level of theory, respectively,²⁹ using the Becke's three-parameter functional in combination with the Lee–Yang–Parr correlation functional (B3LYP)³⁰ and the 6-31G(d,p) basis set.³¹ The vertical excitation and deexcitation energies and the oscillator strengths were calculated by time-dependent density functional theory (TD DFT) with B3LYP functional. For more reliable and comprehensive assignment of the absorption spectra the extended multiconfiguration quasi-degenerate method at the second order of perturbation theory (XMC-QDPT2)³² was also used. Note that the 10 electrons in 10 molecular orbitals (MO) were included in the complete active space of the self-consistent field (CASSCF) approach. State averaged calculations were performed for the systems under investigation with the averaging over the four lowest states and with the effective Hamiltonian including 30 states. Also, the $T_1 \rightarrow T_i$ and $S_1 \rightarrow S_i$ electronic transitions were calculated at the XMC-QDPT2 level of theory with the same conditions. Again, we used the computed wave functions of the singlet and triplet states for calculation of the spin–orbital coupling (SOC) operator matrix elements between these states using the multiconfigurational (MC) SCF treatment in the same active space.

The rate constant of intersystem crossing (k_{ST}) was calculated as³³

$$k_{ST} = 10^{10} \sum_j \sum_{n,m} |\langle \Psi_{S_1} | H_{SO} | \Psi_{T_j} \rangle|^2 F_{nm} \quad (1)$$

where $\langle \Psi_{S_1} | H_{SO} | \Psi_{T_j} \rangle$ (in cm^{-1}) are the matrix elements of spin–orbital coupling operator (H_{SO} is the full Pauli–Breit operator³⁴)

between S_1 state and the j th excited triplet state (T_j) below S_1 , n and m are vibrational quantum numbers of the S_{1n} and T_{jm} vibronic states, F_{nm} are the Franck–Condon factors and $10^{10} \text{ cm}^2 \text{ s}^{-1}$ is the fitting parameter.^{35,36} Note that F_{nm} was calculated in harmonic approximation with all promotive modes and the ezSpectrum software.³⁷ The vibronic spectra were also calculated with the same software including the Dushinsky effect.³⁸

The radiative rate constant (k_r) was calculated according to the well-known equation^{35,36}

$$k_r = \frac{1}{1.5003} f E^2 \quad (2)$$

where f is an oscillator strength for the $S_1 \rightarrow S_0$ electronic transition and E is the de-excitation energy of the transition (cm^{-1}).

The rate constant of internal conversion (k_{IC}) was estimated using the formula^{35,36}

$$\varphi_{fl} = \frac{k_r}{k_r + k_{IC} + k_{S_1 T_i}} \quad (3)$$

where φ_{fl} is the measured fluorescence quantum yield.

All electronic calculations were carried out with Firefly³⁹ and Gamess-US.⁴⁰

C. Synthesis of Solid State Active Media. The active solid media were synthesized using the method which was reported by Costela et al.⁴¹ The mixture of methyl methacrylate (MMA), azobis(isobutyronitrile), and chromenes was used for creation of polymer materials. The chromenes and azobis(isobutyronitrile) were used without additional cleaning and MMA was previously distilled to remove the stabilizer. The solutions were mixed in a chemical shaker in order to achieve complete solubility of the component and then filtered with the 0.2 μm filters, poured into a polyethylene container (the diameter is 20 mm) and purged with argon to remove air. After that, the containers were placed in a water bath with the following regime of temperature changes: the first 2 days, the temperature was maintained at 40 °C, the following 3 days, it was kept at 45 °C, and then every day the temperature rose by 5 °C until it reached 75 °C.

Samples were cooled gradually in the volume and were used to fabricate the laser elements. The machining treatment of the polymer elements was applied with a view to minimize mechanical and thermal stresses.

In the first step, the polymer elements were clamped into a collect holder and then the cylinder (the length is 11 mm) was

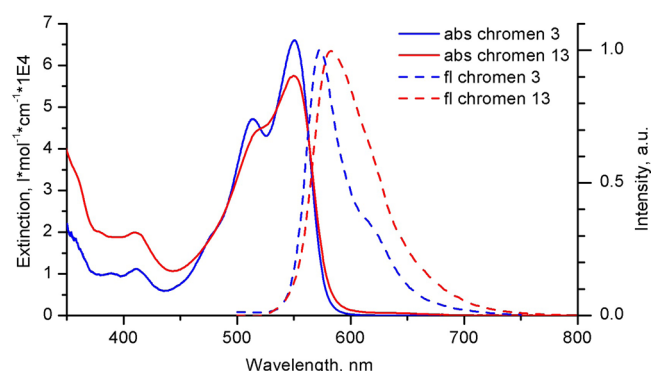


Figure 2. Measured electronic absorption and fluorescence spectra of chromene 3 and chromene 13 in ethanol.

Table 1. Vertical Excitation and De-Excitation Wavelengths (nm) for the Chromene 3 and Chomene 13 Compounds Calculated with TD DFT and XMC-QDPT2 Methods

	chromene 3			chromene 13		
	XMC-QDPT2	TDDFT/B3LYP	exp ^a	XMC-QDPT2	TDDFT/B3LYP	exp ^a
S ₀ → S ₁	454	458	546, ^a 551 ^b	468	473	547, ^a 551 ^b
S ₀ → S ₂	373	401	414 ^b	368	413	410 ^b
S ₁ → S ₀	—	534	561, ^a 573 ^b	—	553	562 ^b 583 ^b

^aMeasure in toluene. ^bMeasure in ethanol.

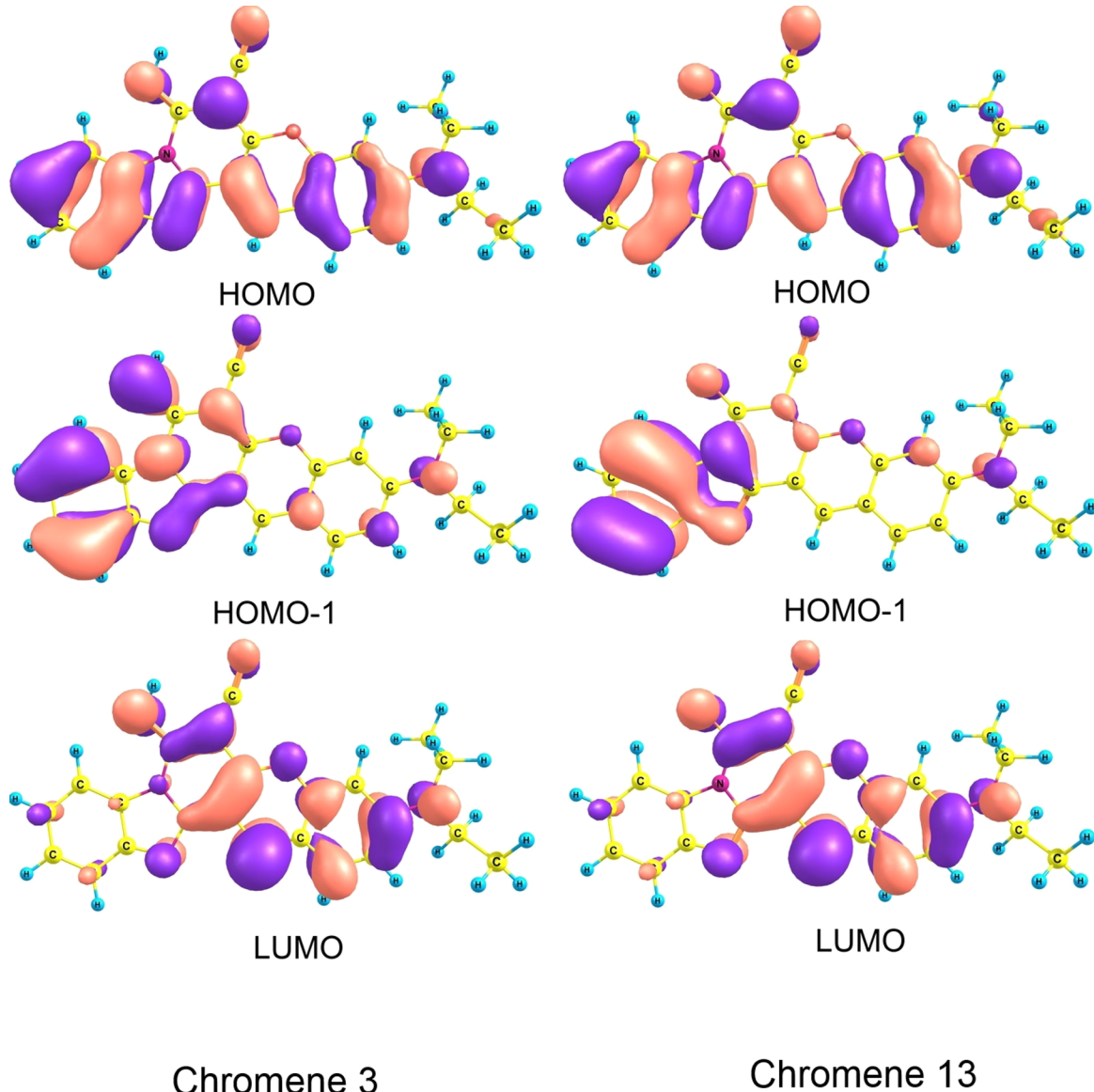


Figure 3. Schematic description of DFT MO for chromene 3 and chromene 13.

cut from the polymer element. This operation was carried out on a lathe with a circular cutter (the thick is 0.5 mm) at 100 rev/min. Note that the operation was carried out without change of the sample mounting to carry to maintain parallelism. The fabricated blanks were polished on the Phoenix 4000 (Buehler) polishing machine. The grinding wheels were used with abrasive size from 50 to 10 μm . The disk rotational speed was 50 rev/min and the pressure of pressing samples was 1 kg/cm². Polishing of the obtained samples was carried out on Trident polishing cloth discs using the diamond paste with a

particle size is 3 μm . The final polishing was carried out on mastertex disks using a polishing liquid with 0.05 μm particle size. The quality of the processing and flatness of the received active samples were tested by the Centaurus microscope and profilometer Thencor MicroXAM 100. The curvature radius of the planes of the working edges of samples did not exceed 0.5 μm .

III. RESULTS AND DISCUSSION

A. Molecular Structure. The optimized S₀ ground state geometry for both chromenes is presented in Figure 1.

The Cartesian coordinates of the optimized geometries for the S_0 and S_1 states are combined in a Supporting Information. Note that the frequency calculation indicates that the found geometries correspond to the real minimum on the potential energy hypersurface since no imaginary frequencies were found. Geometry structures of both dyes are almost planar; deviations from planarity for certain atoms do not exceed 0.1 Å.

B. Electronic Absorption Spectra. The measured electronic absorption spectra of the studied dyes and their fluorescence are presented in Figure 2. As seen from this figure, all spectra of both species are very similar. They have the complicated vibronic structure as the fluorescence spectra have more than one maximum; the first band is located in the range of 573–584 nm for both compounds in ethanol and the second band at 620 nm (well pronounced in chromene 3). The vertical excitation energy (VEE) and de-excitation energies were calculated by TD DDT method. For more sophisticated investigation of the structures and spectra of the considered compounds we use also the XMC-QDPT2 approach. The results are presented in Table 1. Implementation of both methods leads to a similar VEE for the $S_0 \rightarrow S_1$ and $S_0 \rightarrow S_2$ electronic transitions. Also, the comparison of both theoretical and experimental results shows that the first band at 550 nm and the second band at 506–508 nm are formed by the $S_0 \rightarrow S_1$ electronic transition and its vibronic progression, respectively. Note that the calculated VEE values for the $S_0 \rightarrow S_2$ transition are 373 nm (XMC-QDPT2) and 401 nm (TDDFT) for the chromene 3 and 368 nm (XMC-QDPT2) and 413 nm (TDDFT) for the chromene 13 are in a reasonable agreement with the observed weak UV-vis features (Figure 2). Therefore, the $S_0 \rightarrow S_2$ transition cannot form the second band being observed at 506–508 nm of the electronic absorption spectra of the considered compounds. The $S_0 \rightarrow S_2$ transition is responsible for the third band at 400–413 nm. Thus, the theoretical and experimental methods indicate that the second band (506 nm shoulder) of the electronic absorptions spectra of the considered dyes have a vibronic nature.

Our calculations show that the S_1 state is formed by HOMO to LUMO transition (with the weight 0.7) and the S_2 state corresponds to the HOMO-1 \rightarrow LUMO electronic transitions with the weight 0.5 (Figure 3). The $S_0 \rightarrow S_1$ transition includes partial charge transfer from the coumarin part of the dye to the benzoimidazol moiety with considerable excitation in the benzoimidazol moiety. The charge-transfer character explains the red solvent shift and a deviation of the calculated wavelength from the experimental value (Table 1).

The considerable contribution of the excitation in the benzoimidazol part of the dye with the partial charge transfer (Figure 3) provides a large electric dipole transition moment for the first absorption band (the oscillator strength equals to 0.666). Allowed transition character together with a large nuclear displacement in the excited S_1 state determine a well seen vibronic progression in absorption spectra of both dyes. The same reasons are responsible for the lasing ability of chromenes.

C. Vibronic Spectra. The vibronic progression for the $S_0 \rightarrow S_1$ electronic transition were calculated with the Franck–Condon approximation⁴² for the chromene 3 and chromene 13. The simulated vibronic spectra of the considered compounds for the $S_0 \rightarrow S_1$ electronic transition were constructed with the half-width (300 cm^{-1}) at a half-maximum for the convolution of the spectrum using a Gaussian distribution and are presented in Figure 4. The promotive modes are given in Figure 5 and

Figure 6 for the chromene 3 and chromene 13 compounds, respectively.

As seen from Figure 4 there are three noticeable peaks in the chromene 13 absorption spectrum. The first peak is formed by the pure electronic transition (0–0) at 18000 cm^{-1} (553 nm), the second peak is mainly formed by the single excitation of the 1230 cm^{-1} mode (the position of peak is 19230 cm^{-1} or 520 nm) and the third peak is formed by a combination of two singly excited modes 1230 and 1751 cm^{-1} (the position of the peak is at 20981 cm^{-1} or 478 nm). Therefore, the second band of electronic absorption spectrum of chromene 13 (Figure 2) is mainly formed by the singly excited 1230 cm^{-1} mode (C–H in-plane deformation vibrations, Figure 5); the third band seen as a weak twist at 478 nm can be explained as a combined excitation of the 1230 and 1751 cm^{-1} (C=O) vibrational modes.

Figure 6 shows that the promotive modes for chromene 3 are the low-frequency modes ($188, 293, 352, 584, 603 \text{ cm}^{-1}$) and

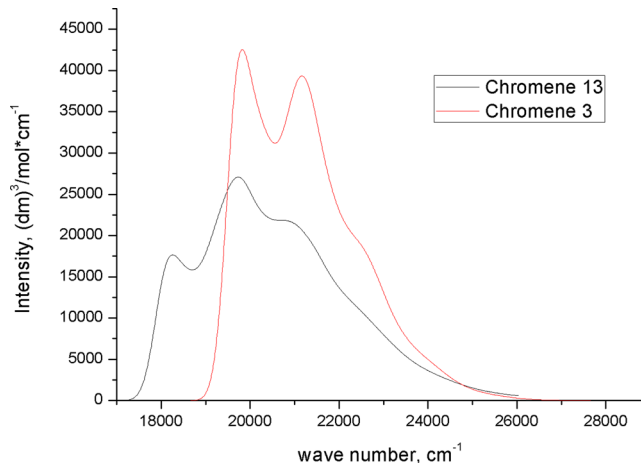


Figure 4. Simulation of vibronic absorption spectra of chromene 3 and chromene 13 dyes.

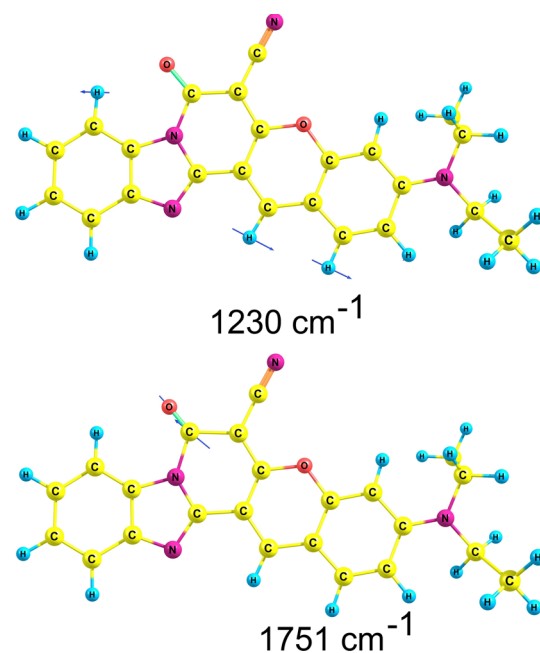


Figure 5. Promotive modes for chromene 13 molecule.

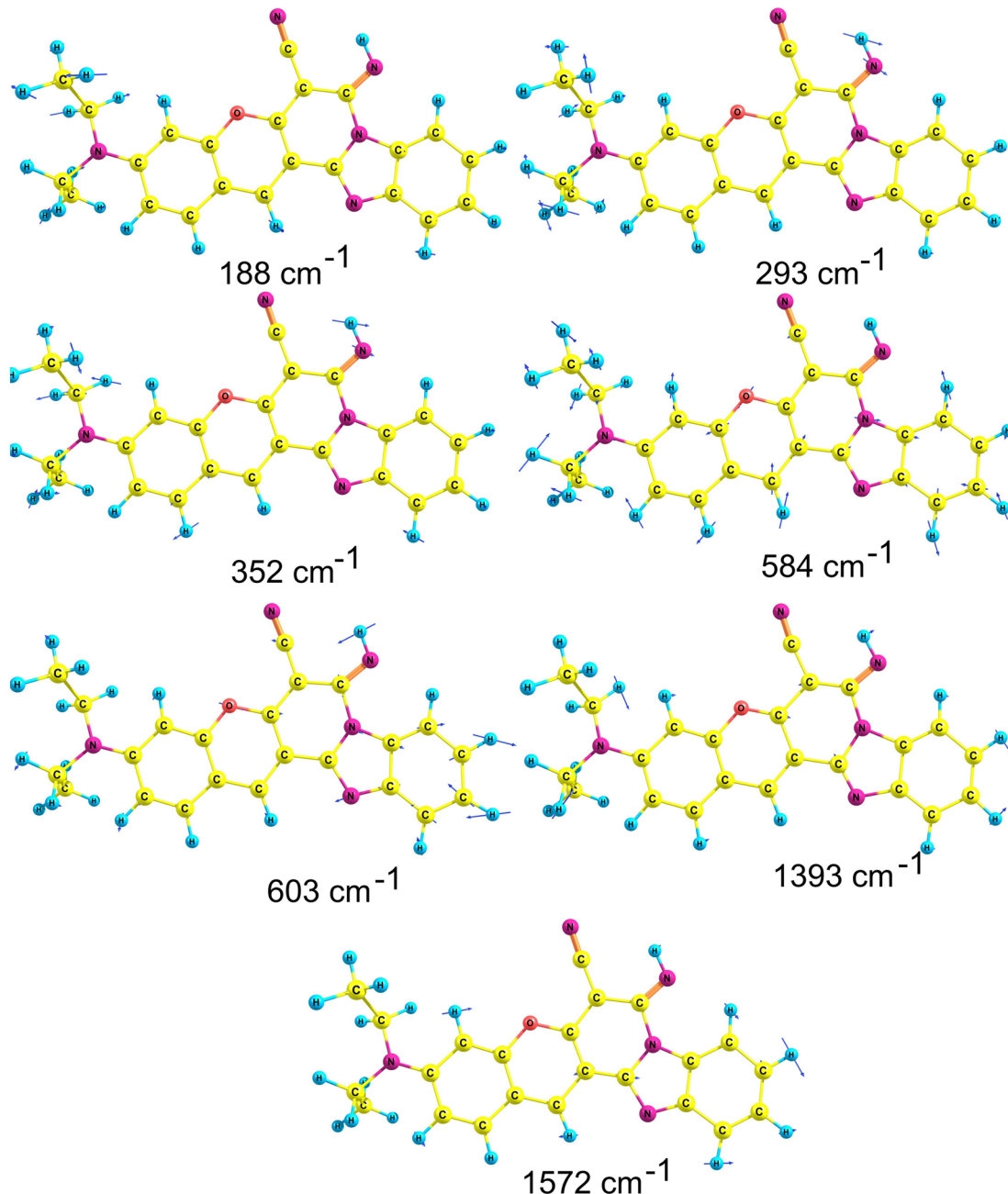


Figure 6. Promotive modes for chromene 3 molecule.

two high-frequency vibrations (1393 and 1572 cm^{-1}). The first peak of the model vibronic spectrum is formed by the pure electronic transition ($0-0$) at 19665 cm^{-1} (508 nm) with a slight broadening (to the right, Figure 4) by the low-frequency vibrations and the second peak (21237 cm^{-1}) is mainly formed by the single excitation of the 1572 cm^{-1} mode (C–H in-plane deformation vibrations again, Figure 6). The higher energy part of the spectrum and a twist at 22500 cm^{-1} (Figure 4) are formed by excitation of combination of modes.

The large difference in the $0-0$ band positions for both dyes (Figure 4) is explained by stronger deformation in the S_1 excited state in chromene 13 connected with the $\text{C}=\text{O}$ group. The similar comparative geometry distortion upon electronic excitations have been calculated for indoline dyes.⁴³ The bad agreement with observed absorption for the predicted $0-0$ band (508 nm) in chromene 3 has the same origin as the poor

agreement for the vertical $S_0 \rightarrow S_1$ excitations (Table 1). In general, the agreement with experiment for emission is much better and quite good. This means that geometry distortion upon $S_0 \rightarrow S_1$ excitation are calculated in a very reliable way. The calculated vibronic activity and Franck–Condon factors are also very reasonable, the late being strongly dependent on distortion upon electronic transition.

Thus, the electronic transition calculations provide a good basement for prediction of the laser generating activity.

D. Photophysical Properties. The calculated photophysical characteristics of chromene 3 and chromene 13 are combined in Table 2 and shown in Figure 7. Note that the measured fluorescence quantum yields in ethanol are 0.99 and 0.75 for the chromene 3 and chromene 13 respectively. They were used for the estimation of k_{IC} for the considered compounds. As seen from Table 2 and Figure 7 the main difference between

Table 2. Computed Spin–Orbit Coupling Matrix Elements, Franck–Condon Factors and Rate Constants for the Photophysical Processes of Chromene 3 and Chromene 13 dyes

	$\langle \Psi_{S_i} H_{SO} \Psi_{T_i} \rangle, \text{ cm}^{-1}$	$\sum_{n,m} F_{nm}$	$k_{ST}, \text{ s}^{-1}$	$k_r, \text{ s}^{-1}$	$k_{IC}, \text{ s}^{-1}$
chromene 3	0.01	10.0	1.2×10^7	4.7×10^8	7.6×10^6
chromene 13	0.01	97.0	1.0×10^8	3.8×10^8	7.0×10^6

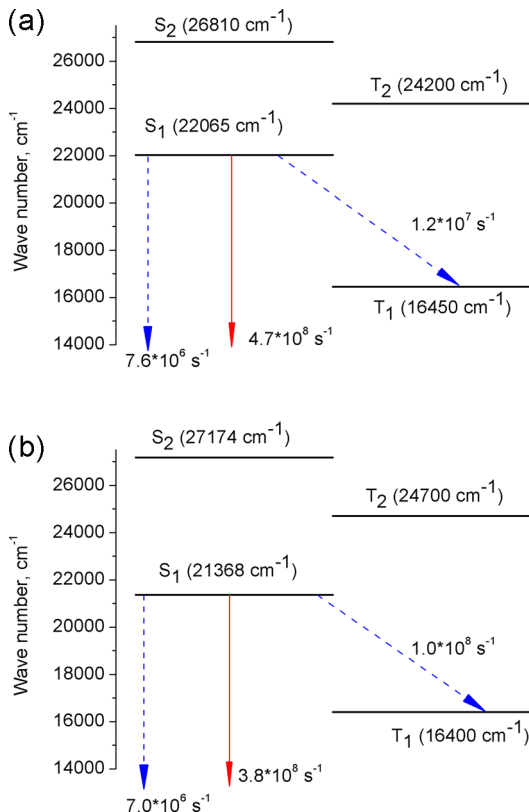


Figure 7. Calculated energy levels (in cm^{-1}) and rate constants (in s^{-1}) for the photophysical processes of chromene 3 (a) and chromene 13 (b) dyes. The red solid arrows and the blue dash arrows illustrate radiation and radiationless deactivation processes, respectively.

the photophysical properties of the investigated molecules is the value of k_{ST} . It is an order of magnitude larger for the chromene 13 in comparison with its value for chromene 3. This fact explains the difference in the fluorescence quantum yields of these compounds. Indeed, the greater the value of intersystem crossing rate constant for the chromene 13 leads to a weaker fluorescence as compared to a chromene 3. Also, the population of T_1 state of chromene 13 is larger than the one for chromene 3.

E. Lasing Properties. The results of the experimental investigation of spectral-luminescence and lasing properties of chromene 3 and chromene 13 are combined in Table 3. It shows that the maximum of lasing wavelengths (609 nm for chromene 3 and 618 nm for chromene 13) are located at the second vibrational peaks of luminescence in toluene. The derivation of lasing on the second peak and not on the first peak, at the transverse pumping, due to the large overlap of the absorption and fluorescence bands. Note that the lasing wavelength of considered molecules is constant at varying concentration of the active substance in a wide range (10^{-4} – 10^{-3} mol/L) in toluene. However, for ethanol, the lasing is located in the long-wave region from the maximum of fluorescence and significantly depends on the concentration of dye. It can be assumed that the main channel of losses during the lasing development is the reabsorption from the ground state. The reason is the strong overlap of absorption and fluorescence spectra. The lasing efficiency of chromene 13 in various solvents is two times lower in comparison with the lasing efficiency of chromene 3. In the work of Valiev et al. it was shown that one of the possible reasons for the low efficiency of lasing of the dye is the induced reabsorption ($T_1 \rightarrow T_i$ and $S_1 \rightarrow S_i$) at the laser wavelength.^{11,44} To confirm this hypothesis we have carried out quantum chemical calculations of $T_1 \rightarrow T_i$ and $S_1 \rightarrow S_i$ absorption spectra using XMC-QDPT2 method. The results of calculations are presented in Table 4. It shows the energies of the $T_1 \rightarrow T_i$ and $S_1 \rightarrow S_i$ transitions with their probability (oscillator strength).

Note that the lasing wavelengths for the chromene 3 and chromene 13 are 609 nm (toluene), 583 nm (ethanol) and 618 nm (toluene), 588 nm (ethanol), respectively (Table 3). The probability of $T_1 \rightarrow T_i$ transitions (with $i = 5, 6, 7$) significantly increases in the chromene 13 in comparison with chromene 3. Also, they are close to the lasing wavelength in ethanol. Note that the population of T_1 state of chromene 13 is larger than the one of chromene 3 according to Table 2. Therefore, the calculations (Tables 4 and 2) show that the induced reabsorption ($T_1 \rightarrow T_i$ and $S_1 \rightarrow S_i$) at the laser wavelength can be the reason for the small lasing efficiency of chromene 13 in comparison with one of chromene 3.

F. Solid Active Media. The next step of investigation of the chromene molecules is the creation of solid active media based on their introduction into the polymethyl metacrylate (PMMA)

Table 3. Spectral-Luminescence and Lasing Properties of Chromene 3 and Chromene 13 Molecules

compound	solvent	$\lambda_{\text{abs}}, \text{ nm}$	$\epsilon, \text{ M}^{-1} \text{ cm}^{-1}$	$\lambda_{\text{fl}}, \text{ nm}$	$\Delta\nu_{\text{stokes}}, \text{ cm}^{-1}$	QY, %	$\lambda_{\text{las}}^a, \text{ nm}$	efficiency, ^a %
chromene 3	toluene	507	61000	561, 606	490	0.95	609	40
		546	61000					
	ethanol	514	47100	573	700	0.99	583	36
		551	66000					
chromene 13	toluene	510	51000	562, 607	490	0.78	618	23
		547	51000					
	ethanol	516	43900	583	1000	0.75	588	20
		551	57500					

^aLasing properties are given at a concentration of 2×10^{-4} mol/L.

Table 4. Excitation Energies (cm^{-1}) and Oscillator Strengths (f) for the $S_1 \rightarrow S_n$ and $T_1 \rightarrow T_n$ Electronic Transitions of Chromene 3 and Chromene 13 Compounds Calculated by XMC-QDPT2 Level of Theory

Chromene 3			
$S_1 \rightarrow S_n$	$E(f)$	$T_1 \rightarrow T_n$	$E(f)$
$S_1 \rightarrow S_2$	1136(0.13)	$T_1 \rightarrow T_2$	729(0.1)
$S_1 \rightarrow S_3$	819(0.001)	$T_1 \rightarrow T_3$	692(0.02)
$S_1 \rightarrow S_4$	680(7×10^{-4})	$T_1 \rightarrow T_4$	630(0.1)
$S_1 \rightarrow S_5$	606(0.07)	$T_1 \rightarrow T_5$	562(0.07)
$S_1 \rightarrow S_6$	537(0.05)	$T_1 \rightarrow T_6$	518(0.2)
$S_1 \rightarrow S_7$	518(0.04)	$T_1 \rightarrow T_7$	505(0.07)
$S_1 \rightarrow S_8$	473(1.23)	$T_1 \rightarrow T_8$	426(0.3)
$S_1 \rightarrow S_9$	429(0.003)	$T_1 \rightarrow T_9$	403(0.02)
$S_1 \rightarrow S_{10}$	399(0.17)	$T_1 \rightarrow T_{10}$	385(0.004)

Chromene 13			
$S_1 \rightarrow S_n$	$E(f)$	$T_1 \rightarrow T_n$	$E(f)$
$S_1 \rightarrow S_2$	1035(0.14)	$T_1 \rightarrow T_2$	870(0.14)
$S_1 \rightarrow S_3$	808(0.02)	$T_1 \rightarrow T_3$	700(0.03)
$S_1 \rightarrow S_4$	661(0.004)	$T_1 \rightarrow T_4$	645(0.003)
$S_1 \rightarrow S_5$	583(0.08)	$T_1 \rightarrow T_5$	564(0.40)
$S_1 \rightarrow S_6$	525(0.03)	$T_1 \rightarrow T_6$	529(0.001)
$S_1 \rightarrow S_7$	505(0.009)	$T_1 \rightarrow T_7$	507(0.21)
$S_1 \rightarrow S_8$	461(1.4)	$T_1 \rightarrow T_8$	456(0.003)
$S_1 \rightarrow S_9$	423(0.03)	$T_1 \rightarrow T_9$	418(0.03)
$S_1 \rightarrow S_{10}$	389(0.10)	$T_1 \rightarrow T_{10}$	385(0.07)

matrix. Lasing efficiency of chromene 3 in solution and in PMMA matrix is close to 40–45% and that of chromene 13 is equal to 20% in solution and 16%—in the matrix. Lasing generation for both molecules is obtained at 605–607 nm near the second vibrational peak.

Figure 8 presents the dependence of the lasing efficiency of the pump power density. In solutions the efficiency curve of the

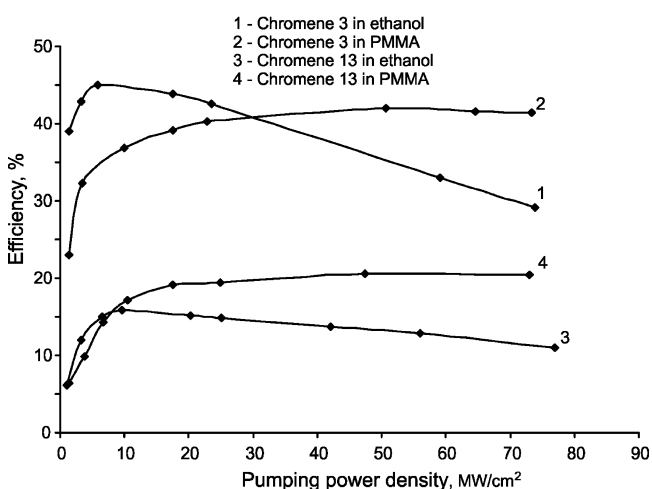


Figure 8. Dependence of the lasing efficiency on the pump power density.

power density goes through a maximum at 8–10 MW/cm² and then, the efficiency decreases with increasing pump. In solid samples in PMMA the lasing efficiency does not depend on the pump intensity after 15–20 MW/cm². This difference is explained by formation of a thermal lens in the solution, which is appeared by the change of the refractive index of the solvent

due to the temperature rise in the pump region. After termination of the excitation pulse, the solution is mixed due to the Brownian motion. In PMMA matrices this effect is not observed because the temperature coefficient of the refractive index for PMMA ($-1.13 \times 10^{-4} \text{ K}^{-1}$)⁴⁵ is 4 times lower than that for ethanol ($-4 \times 10^{-4} \text{ K}^{-1}$).⁴⁶ Clearly, the appearance of a thermal lens leads to defocusing of light emission and therefore leads to decrease of lasing efficiency of the solution.

It should be noted that the solid active media possess the high photostability. The dependence of the efficiency on the number of pump pulses in one area of the active medium is given in Figure 9. It can be seen that the number of pulses is

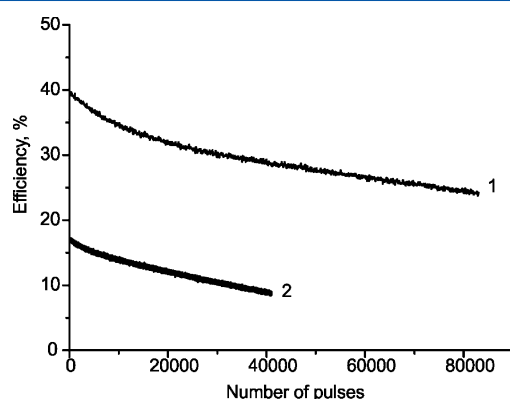


Figure 9. Dependence of the lasing efficiency on the number of excitation pulses in one area of the active medium: (1) chromene 3; (2) chromene 13.

80000 counts when a decline in efficiency of 38% of the initial value for chromene 3. The photostability of chromene 13 is less than that for chromene 3 (the number of pulses is 40000 pulses when efficiency is reduced by 50% from initial value). However, the quality of solid-state sample requires optimization, and this work can be continued.

It should be noted that the conversion efficiency of considered molecules is not optimized to the Q-factor of the resonator and will be corrected in further investigation. For example, the replacement of the nonselective aluminum mirror on dielectric one with a high reflection coefficient (~100%) at the laser wavelength leads to an increase of lasing efficiency of chromene 13 from 20% to 28% in solutions.

IV. CONCLUSION

In this work, we have studied by theory and by experiment the spectral-luminescent and lasing properties of the chosen chromene dyes. TD DFT calculation predicts geometry distortion upon electronic excitation and provides a good simulation of vibronic activity in the absorption spectra. On the bases of the synthesized polymethyl metacrylate matrix doped by chromenes we have created the laser active media with high efficiency and long operation time. It has been shown that the cause of reduction of lasing efficiency of chromene 13 in comparison with chromene 3 are both high value of k_{ST} and the $T_1 \rightarrow T_i$ reabsorption at the lasing wavelength.

It is shown that the laser efficiency and operation time of the chromene 3 dye in solvent and in matrices is higher than those of the chromene 13 which is explained by the larger structural distortion upon electronic transition.

■ ASSOCIATED CONTENT

§ Supporting Information

Cartesian coordinates of atoms in the equilibrium geometries of the different electronic states and their main vibrational modes of chromene 3 and chromene 13. This material is available free of charge via the Internet at <http://pubs.acs.org>.

■ AUTHOR INFORMATION

Corresponding Author

*(R.R.V.) Telephone: +73822-529-640. Fax: +73822-529-651. E-mail: valiev_rashid@mail.ru.

Notes

The authors declare no competing financial interest.

■ ACKNOWLEDGMENTS

The work is performed in the framework of the RF state program 16.578.2014/K. Also, we thank Dr. Lubov Savvina from NIOPIK for the provided dyes. We are grateful to Dr. Alexandra Ya. Freidzon for the useful discussion.

■ REFERENCES

- (1) Somasundaram, G.; Ramalingam, A. Gain studies of Coumarin 490 dye-doped polymer laser. *Chem. Phys. Lett.* **2000**, *324*, 25–30.
- (2) Somasundaram, G.; Ramalingam, A. Gain studies of Coumarin 1 dye-doped polymer laser. *J. Lumin.* **2000**, *90*, 1–5.
- (3) Somasundaram, G.; Ramalingam, A. Gain studies of Coumarin 307 dye doped polymer laser. *Opt. Laser Technol.* **1999**, *31*, 351–358.
- (4) Somasundaram, G.; Ramalingam, A. Gain studies of Coumarin 503 dye-doped polymer laser. *Opt. Lasers Eng.* **2000**, *33*, 157–163.
- (5) Duran-Sampedro, G.; Esnal, I.; Agarrabeitia, A. R.; Bañuelos Prieto, J.; Cerdán, L.; García-Moreno, I.; Costela, A.; Lopez-Arbeloa, I.; Ortiz, M. J. First highly efficient and photostable E and C derivatives of 4,4-Difluoro-4-bora-3a,4a-diaza-s-indacene (BODIPY) as dye lasers in the liquid phase, thin films, and solid-state rods. *Chem.—Eur. J.* **2014**, *20*, 2646–2653.
- (6) Gartzia-Rivero, Y.; Bañuelos, J.; López-Arbeloa, I.; Costela, A.; García-Moreno, I.; Xiao, Y. Photophysical and laser properties of cassettes based on a BODIPY and Rhodamine pair. *Chem.—Asian J.* **2013**, *8*, 3133–3141.
- (7) Durán-Sampedro, G.; Agarrabeitia, A. R.; Cerdán, L.; Pérez-Ojeda, M. E.; Costela, A.; García-Moreno, I.; Esnal, I.; Bañuelos, J.; Arbeloa, I. L.; Ortiz, M. J. Carboxylates versus Fluorines: boosting the emission properties of commercial BODIPYs in liquid and solid media. *Adv. Funct. Mater.* **2013**, *23*, 4195–4205.
- (8) Duran-Sampedro, G.; Agarrabeitia, A. R.; Garcia-Moreno, I.; Costela, A.; Bañuelos, J.; Arbeloa, T.; Arbeloa, I. L.; Chiara, J. L.; Ortiz, M. J. Chlorinated BODIPYs: surprisingly efficient and highly photostable laser dyes. *Eur. J. Org. Chem.* **2012**, *32*, 6335–6350.
- (9) Kopylova, T. N.; Maier, G. V.; Solodova, T. A.; Tel'minov, E. N.; Eremina, N. S.; Vaitulevich, E. A.; Samsonova, L. G.; Solodov, A. M. Active media for tunable lasers based on hybrid polymers. *Quantum Electron.* **2008**, *38*, 109–114.
- (10) Kopylova, T. N.; Anufrik, S. S.; Mayer, G. V.; Solodova, T. A.; Tel'minov, E. N.; Degtyarenko, K. M.; Samsonova, L. G.; Gadirov, R. M.; Nikonorov, S.Yu.; Ponyavina, E. N.; et al. Investigation of characteristics of solid-state active media based on pyrromethene 567. *Russ. Phys. J.* **2013**, *55*, 1137–1142.
- (11) Valiev, R. R.; Tel'minov, E. N.; Solodova, T. N.; Ponyavina, E. N.; Gadirov, R. M.; Mayer, G. V.; Kopylova, T. N. Lasing of pyrromethene 567 in solid matrices. *Chem. Phys. Lett.* **2013**, *588*, 184–187.
- (12) Ortiz, M. J.; Garcia-Moreno, I.; Agarrabeitia, A. R.; Duran-Sampedro, G.; Costela, A.; Sastre, R.; Arbeloa, F. L.; Prieto, J. B.; Arbeloa, I. L. Red-edge-wavelength finely-tunable laser action from new BODIPY dyes. *Phys. Chem. Chem. Phys.* **2010**, *12*, 7804–7811.
- (13) Tyagia, A.; Aguua, D. del; Penzkofer, A.; García, O.; Sastre, R.; Costela, A.; García-Moreno, I. Photophysical characterization of pyrromethene 597 laser dye in cross-linked silicon-containing organic copolymers. *Chem. Phys.* **2007**, *342*, 201–214.
- (14) García, O.; Garrido, L.; Sastre, R.; Costela, A.; García-Moreno, I. Synthetic strategies for hybrid materials to improve properties for optoelectronic applications. *Adv. Funct. Mater.* **2008**, *18*, 2017–2025.
- (15) Costela, A.; García-Moreno, I.; Barroso, J.; Sastre, R. Laser performance of pyrromethene 567 dye in solid matrices of methyl methacrylate with different comonomers. *Appl. Phys. B: Laser Opt.* **2000**, *70*, 367–373.
- (16) García, O.; Sastre, R.; Agua, D.; del Costela, A.; García-Moreno, I.; López Arbeloa, F.; Prieto, J. B.; Arbeloa, I. L. Laser and physical properties of bodipy chromophores in new fluorinated polymeric materials. *J. Phys. Chem. C* **2007**, *111*, 1508–1516.
- (17) García-Moreno, I.; Costela, A.; Pintado-Sierra, M.; Martin, V.; Sastre, R. Enhanced laser action of Perylene-Red doped polymeric materials. *Opt. Express* **2009**, *17*, 12777–12784.
- (18) García-Moreno, I.; Costela, A.; Martin, V.; Pintado-Sierra, M.; Sastre, R. Materials for a reliable solid-state dye laser at the red spectral edge. *Adv. Funct. Mater.* **2009**, *19*, 2547–2552.
- (19) García-Moreno, I.; Costela, A.; Pintado-Sierra, M.; Martin, V.; Sastre, R. Efficient red-edge materials photosensitized by rhodamine 640. *J. Phys. Chem. B* **2009**, *113*, 10611–10618.
- (20) Costela, A.; García-Moreno, I.; Gomez, C.; García, O.; Sastre, R. New organic–inorganic hybrid matrices doped with rhodamine 6G as solid-state dye lasers. *Appl. Phys. B: Laser Opt.* **2002**, *75*, 827–833.
- (21) Costela, A.; García-Moreno, I.; García, O.; Agua, D. Del; Sastre, R. Structural influence of the inorganic network in the laser performance of dye-doped hybrid materials. *Appl. Phys. B: Laser Opt.* **2005**, *80*, 749–755.
- (22) Sastre, R.; Martín, V.; Garrido, L.; Chiara, J. L.; Trastoy, B.; García, O.; Costela, A.; García-Moreno, I. Dye-doped polyhedral oligomeric silsesquioxane (poss)-modified polymeric matrices for highly efficient and photostable solid-state lasers. *Adv. Funct. Mater.* **2009**, *19*, 3307–3316.
- (23) Costela, A.; García-Moreno, I.; Cerdan, L.; Martin, V.; García, O.; Sastre, R. Dye-doped poss solutions: random nanomaterials for laser emission. *Adv. Funct. Mater.* **2009**, *21*, 4163–4166.
- (24) Aldag, H. R.; Dolotov, S. M.; Koldunov, M. F.; Kravchenko, Ya.V.; Manenkov, A. A.; Pacheco, D. P.; Ponomarenko, E. P.; Reznichenko, A. V.; Roskova, G. P.; Tsekhomskayam, T. S. A microporous glass-polymer composite as a new material for solid-state dye lasers: II. Lasing properties. *Quantum Electron.* **2000**, *30*, 1055.
- (25) García-Moreno, I.; Costela, A.; García, O.; Auga, D. del; Sastre, R. Synthesis, structure, and physical properties of hybrid nanocomposites for solid-state dye lasers. *J. Phys. Chem. B* **2005**, *109*, 21618–21626.
- (26) Ismael, R.; Schwander, H.; Hendrix, P. *Ullmann's Encyclopedia of Industrial Chemistry*; Wiley: New York, 2013; pp 1–22.
- (27) Wang, W.; Xu, L.; Liu, F.; Li, X. Synthesis of isocyanate microcapsules and micromechanical behavior improvement of microcapsule shells by oxygen plasma treated carbon nanotubes. *J. Mater. Chem. A* **2013**, *1*, 776–782.
- (28) Maslov, V. V.; Nikitchenko, V. M. Dual-band lasing of benzopyran dyes in the red region of the spectrum. *J. Appl. Spectrosc.* **2006**, *73*, 454–457.
- (29) Casida. *Recent Advances in Density Functional Methods Part I*; World Scientific: Singapore, 1999; pp 155–192.
- (30) Lee, C.; Yang, W.; Parr, R. G. Development of the Colle-Salvetti correlation-energy formula into a functional of the electron density. *Phys. Rev. B: Condens. Matter Mater. Phys.* **1988**, *37*, 785–789.
- (31) Rassolov, V.; Pople, J. A.; Ratner, M.; Windus, T. L. 6-31G* basis set for atoms K through Zn. *J. Chem. Phys.* **1998**, *109*, 1223.
- (32) Granovsky, A. A. Extended multi-configuration quasi-degenerate perturbation theory: The new approach to multi-state multi-reference perturbation theory. *J. Chem. Phys.* **2011**, *134*, 214113.
- (33) McGlynn, S. P.; Azumi, T.; Kinoshita, M. *Molecular spectroscopy of the triplet state*; Prentice-Hall: Englewood Cliffs, NJ, 1969; p 28

- (34) Fedorov, D. G.; Koseki, S.; Schmidt, M. W.; Gordon, M. S. Spin-orbit coupling in molecules: chemistry beyond the adiabatic approximation. *Int. Rev. Phys. Chem.* **2003**, *22*, 551–592.
- (35) Plotnikov, V. G.; Dolgikh, V. A.; Komarov, V. M. Processes of internal conversion in aromatic impurity molecules. *Opt. Spectrosc.* **1977**, *43*, 522–527.
- (36) Valiev, R. R.; Cherepanov, V. N.; Artyukhov, V.Ya.; Sundholm, D. Computational studies of photophysical properties of porphin, tetraphenylporphyrin and tetrabenzo porphyrin. *Phys. Chem. Chem. Phys.* **2012**, *14*, 11508–11517.
- (37) Mozhayskiy, V. A. and Krylov, A. I. *ezSpectrum*, <http://iopenshell.usc.edu/downloads>.
- (38) Duschinsky, F. *Acta Physicochim. URSS* **1937**, *7*, 551.
- (39) Granovsky, A. A. *Firefly*, version 8.0.0, <http://classic.chem.msu.su/gran/firefly/index.html>.
- (40) Schmidt, M. W.; Baldridge, K. K.; Boatz, J. A.; Elbert, S. T.; Gordon, M. S.; Jensen, J. H.; Koseki, S.; Matsunaga, N.; Nguyen, K. A.; Su, S.; et al. General Atomic and Molecular Electronic Structure System. *J. Comput. Chem.* **2006**, *14*, 1347–1363.
- (41) Costela, A.; Garcia-Moreno, I.; Sastre, R. Polymeric solid-state dye lasers: Recent developments. *Phys. Chem. Chem. Phys.* **2003**, *5*, 4745–4763.
- (42) Minaev, B.; Wang, Y.-H.; Wang, C.-K.; Luo, Y.; Agren, H. Density functional theory study of vibronic structure of the first absorption Q_x band in free-base porphin. *Spectrochim. Acta, Part A* **2006**, *65*, 308–323.
- (43) Baryshnikov, G. V.; Minaev, B. F.; Minaeva, V. A. Quantum-chemical study of the structure and optical properties of sensitized dyes of an indoline-thiazolidine series. *Opt. Spectrosc.* **2010**, *108*, 16–22.
- (44) Valiev, R. R.; Sinelnikov, A. N.; Aksanova, Y. V.; Kuznetsova, R. T.; Berezin, M. B.; Semeikin, A. S.; Cherepanov, V. N. The computational and experimental investigations of photophysical and spectroscopic properties of BF₂ dipyromethene complexes. *Spectrochim. Acta, Part A* **2014**, *117*, 323–329.
- (45) Kang, E.-S.; Bae, J. Y.; Bae, B.-S. Measurement of thermo-optic coefficients in sol-gel hybrid glass films. *J. Sol-Gel Sci. Technol.* **2003**, *26*, 981–984.
- (46) Jimenez Rioboo, R. J.; Philipp, M.; Ramos, M. A.; Kruger, J. K. Concentration and temperature dependence of the refractive index of ethanol-water mixtures: Influence of intermolecular interactions. *Eur. Phys. J. E* **2009**, *30*, 19–26.